Study of the Λp Interaction Close to the $\Sigma^+ n$ and $\Sigma^0 p$ Thresholds

H. Machner,[1] J. Haidenbauer,[2,3] F. Hinterberger,[4]
A. Magiera,[5] J.A. Niskanen,[6] J. Ritman,[2] R. Siudak[7]

[1]Fachbereich Physik, Universität Duisburg-Essen,
Duisburg, Germany
[2]Institut für Kernphysik and Jülich Centre for Hadron Physics,
Forschungszentrum Jülich, Jülich, Germany
[3]Institute for Advanced Simulation,
Forschungszentrum Jülich, Jülich, Germany
[4]Helmholtz-Institut für Strahlen- und Kernphysik
der Universität Bonn, Bonn, Germany
[5]Institute of Physics, Jagellonian University,
Kraków, Poland
[6]Department of Physical Sciences, University of Helsinki,
Helsinki, Finland
[7]Institute of Nuclear Physics, Polish Academy of Sciences,
Kraków, Poland

January 28, 2013

Abstract

The Λp interaction close to the ΣN threshold is considered. Specifically, the pronounced structure seen in production reactions like $K^- d \to \pi^- \Lambda p$ and $pp \to K^+ \Lambda p$ around the ΣN threshold is analyzed. Modern interaction models of the coupled $\Lambda N - \Sigma N$ systems generate such a structure either due to the presence of a (deuteron-like) unstable bound state or of an inelastic virtual state. A determination of the position of the prominent peak as observed in various experiments for the two aforementioned reactions leads to values that agree quite well with each other. Furthermore, the deduced mean value of 2128.7 ± 0.3 MeV for the peak position coincides practically with the threshold energy of the $\Sigma^+ n$ channel. This supports the interpretation of the structure as a genuine cusp, signaling an inelastic virtual state in the $^3S_1 - ^3D_1$ partial wave of the ΣN isospin $1/2$ channel. There is also evidence for a second peak (or shoulder) in the data sets considered which appears at roughly 10-15 MeV above the ΣN

threshold. However, its concrete position varies significantly from data set to data set and, thus, a theoretical interpretation is difficult.

1 Introduction

Since the discovery of strangeness, the hyperon–nucleon (YN) interaction has been of fundamental interest both theoretically [1] as well as experimentally [2]. First, its knowledge is important for the general understanding of the structure of hadrons and their constituents. Further, it is also needed to explain the spectra of hypernuclei, which, in return, also convey information on these interactions especially at small relative energies. Unfortunately, since hyperons are short lived, this energy region is practically inaccessible by hyperon beams. Thus, possible bound states are indispensable as the source of information. In this report we will concentrate on the Λp interaction at energies close to the threshold of the ΣN channels. These are at 2128.94 MeV (for $\Sigma^+ n$) and at 2130.9 MeV (for $\Sigma^0 p$). In this region experimental data for elastic scattering,

$$\Lambda p \to \Lambda p \ , \tag{1}$$

indicate an enhancement in the Λp cross section as we will discuss in the next sections. However, the dynamical origin of this enhancement remains unclear so far. It could be a cusp structure due to (and at) the opening of the ΣN threshold and then would be a signal for an inelastic virtual state (we follow here the nomenclature used and explained in Ref. [3]) or due to a bound $\Sigma^0 p$ or $\Sigma^+ n$ state, i. e. a deuteron-like but unstable bound state. In the latter case the peak of the cross section has to be below the ΣN threshold. In principle, it could also be a Λp resonance above the ΣN threshold.

Data from elastic scattering experiments that cover this range exist in the literature, but so far the momentum resolution of the Λ beams has been insufficient to draw firm conclusions. A much more promising avenue is offered by the study of final state interactions (FSI). Assuming relative weakness of the pion interaction one possibility is the strangeness exchange reaction

$$K^- d \to \pi^- \Lambda p. \tag{2}$$

Also strangeness production processes like

$$\pi^+ d \to K^+ \Lambda p \tag{3}$$

$$pp \to K^+ \Lambda p \tag{4}$$

should contain basically the same information.

In this work we will concentrate on the two reactions (2) and (4). With regard to the former reaction, evidence for an enhancement in the Λp cross section near the ΣN threshold has been already found in the late 1960s and confirmed in later experiments [4–10]. We review those data and we also re-analyze them with the aim to determine accurately the position of this enhancement. Experimental information about the reaction 4, in the region of the ΣN threshold,

has become available much more recently and clear evidence for the presence of an enhancement at that threshold is only emerging right now. Here we perform an analysis of data from the inclusive measurements of the reaction $pp \to K^+X$ performed at Saclay [11] and in Jülich [12], respectively, and attempt to extract the enhancement and its position from those experiments too. This sort of analysis suffers from lacking precise pp *exclusive* data to rely on. However, as we will see, the positions determined from the two reactions (2) and (4) agree with each other, and they also coincide with the opening of the Σ^+n channel within the error bars of our analysis.

We also study an additional peak (or shoulder) that is present in basically all the aforementioned measurements and located a few MeV above the ΣN threshold. However, in this case it turns out that there are sizable variations of its position between reaction (2) and (4), but even between measurements of one and the same reaction. Thus, the physical significance of that peak remains unclear to some extent.

The paper is organized as follows. In the next section we take a look at the status of the results from elastic Λp scattering. We discuss also the behavior of the Λp cross section around the ΣN threshold as predicted by various YN interaction models from the literature. In the two subsequent sections the data for the two reactions (2) and (4) are discussed. In section 5 the peak structures found are analyzed. In particular, we determine their position as seen in the various measurements for the two reactions in question. The paper ends with a summary.

2   Elastic Λp Scattering

Before discussing the situation for ΛN scattering let us briefly recall some well-known features of coupled-channels dynamics [3, 13]. Conservation of flux and the associated unitarity of the S-matrix necessarily imply anomalies at the opening of new thresholds [13]. Specifically, at an S-wave threshold the cross section of the "old" channel as a function of the energy will, in general, have infinite slopes at such a threshold. The resulting structures are usually called cusps or rounded steps, depending on their specific shape [3, 13]. Whether these structures remain primarily of academic interest or manifest themselves via large, experimentally observable effects depends strongly on the strengths of the interactions in the coupled channels. In particular, pronounced threshold phenomena always go along with near-by poles in the scattering amplitudes of the involved channels that are associated with (inelastic) virtual states or (unstable) bound states [3, 14].

Modern meson-exchange models of the YN interaction such as the Jülich [15, 16] or Nijmegen potentials [17, 18] are derived under the assumption of (broken) SU(3) symmetry. This symmetry implies, that the strongly attractive forces that yield the deuteron bound state (in the $^3S_1 - {}^3D_1$ partial wave) and a virtual state in the $^1S_0$ partial wave in case of the NN system will likewise act in the strangeness $S = -1$ sector (see, e.g., Refs. [19, 20] for details on the
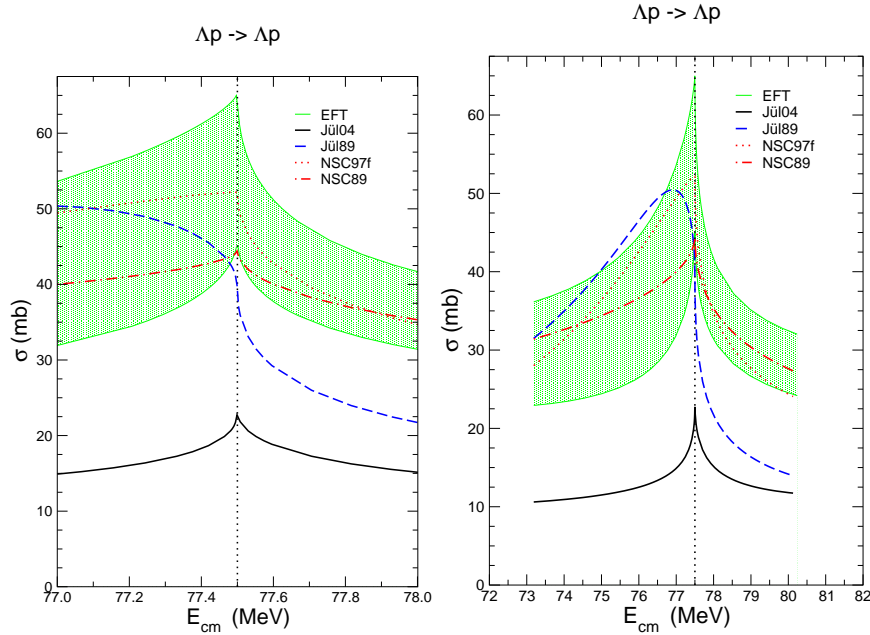
Figure 1: Elastic ΛN cross section as function of the center-of-mass energy. Jül04 and Jül89 are results for the Jülich potentials published in Refs. [15] and [16], respectively. NSC97f and NSC89 refer to results of the corresponding Nijmegen soft-core potentials [17] and [18]. Results obtained at leading-order chiral EFT [19, 20] are indicated by the grey band. The dashed line is the threshold for the $\Lambda p \to \Sigma N$ transition. The left part has an expanded energy scale.

SU(3) relations). Specifically, there is a strong coupling between the ΛN and ΣN systems. It is caused by the long-ranged tensor force provided by pion exchange and boosted by the fact that the thresholds of the two channels are only separated by 77 MeV. Therefore, it is not surprising that practically all YN interactions that fit the data and include explicitly the coupling between the ΛN and ΣN channels predict also sizeable threshold effects.

A closer inspection of the results for published interaction models reveals that, in general, they can be grouped into two categories. In one case the predicted ΛN cross section around the ΣN threshold is in the order of 40 to 50 mb and, more characteristic, roughly a factor four larger than a few MeV away from the threshold. The cross section is so large because one of the eigenphases of the tensor-coupled $^3S_1 - ^3D_1$ partial wave (in most cases the $^3D_1$) passes through 90° right below the ΣN threshold. Due to the latter aspect, the peak of the cross section is actually not at the ΣN threshold but slightly below. Thus, in this case the ΛN cross section exhibits a typical resonance-like behavior.

4

Moreover, no cusp appears at the actual ΣN threshold, only a rounded step [3, 13]. However, since the peak of the cross section occurs so close to the ΣN threshold – often the separation is less than an MeV – it is usually impossible to recognize the above features in the published results due to the scale used for the figures! Pole searches performed for the amplitudes produced by the potential models in question found that these are located in the second quadrant of the complex plane of the relative momentum in the ΣN channel [14]. Thus, these YN interactions are characterized by the presence of an unstable bound state, i.e. a deuteron-like ΣN state [3]. The Nijmegen potentials NSC97f [17] and NF [21] but also the original Jülich YN interaction [16] belong to this category. In the case of an unstable bound state it is also possible that the $^3S_1$ eigenphase passes through $90°$ (instead of the $^3D_1$). Interestingly, such a scenario is seldom realized. In fact, we are aware of only one meson-exchange YN potential where this happens, namely the Nijmegen ESC04 interaction [22]. In case of the interactions considered in [23] it is also the $^3S_1$ that passes through $90°$. But since these potentials were intended for application in Faddeev-type calculations for simplicity reasons only S-waves were taken into account. One of the interactions considered in [23] has the rather unique feature that the predicted $^3S_1$ phase passes through $90°$ slightly above the ΣN threshold. As far as we can see, this does not happen for any of the meson-exchange YN potentials whose phase shifts are documented in the literature.

The second category of YN potentials produces a peak in the ΛN cross section precisely at the ΣN threshold. Thus, now we do observe a genuine threshold cusp. Here none of the relevant eigenphases passes through $90°$. In general the ΛN cross section at the ΣN threshold is roughly a factor two larger than at a few MeV away from the threshold. Usually, the peak values are around 20 mb, but can still reach up to 40 mb. The poles for this kind of potentials are located in the third quadrant of the complex plane of the relative momentum in the ΣN channel [14]. They are an indication for the presence of inelastic virtual states [3], i.e. the analog of the virtual state in the NN $^1S_0$ partial wave. The Nijmegen potentials ND [24], NSC89 [18] and ESC08 [25], and also the recent Jülich YN interaction [15] belong to this category. Also a YN interaction derived at leading-order in chiral effective field theory (EFT) [19, 20] predicts such a behavior.

In order to illustrate the statements made above, Λp cross sections for the Nijmegen soft-core potentials NSC97f [17] and NSC89 [18], and for the Jülich potentials from 2005 [15] and 1989 [16] are shown in Fig. 1 for energies around the ΣN threshold for two different energy scales. Results obtained at leading-order chiral EFT [19, 20] are indicated by the grey band. One can see that the cross sections predicted by those YN potentials indeed exhibit different features at the ΣN threshold. As said above the Nijmegen NSC97f and the Jülich 1989 one-boson exchange models produce a deuteron-like unstable bound state in the ΣN channel. In both cases the $^3D_1$ ΛN phase shift shows a resonance-like behavior and crosses $90°$ slightly below the ΣN threshold [15, 19]. The rounded step in the cross section of the Jül89 potential is clearly visible in the left figure (with magnified scale). The structure produced by the NSC97f potential is

similar. However, since in this case (in our calculation) the $^3D_1$ phase shift crosses $90°$ at a mere 20 keV below the nominal ΣN threshold a further increase in the scale would be required to see that. The Jül04 and the NSC89 models and the EFT interaction support an inelastic virtual state rather than a bound state and, consequently, a genuine cusp structure appears in the cross section.
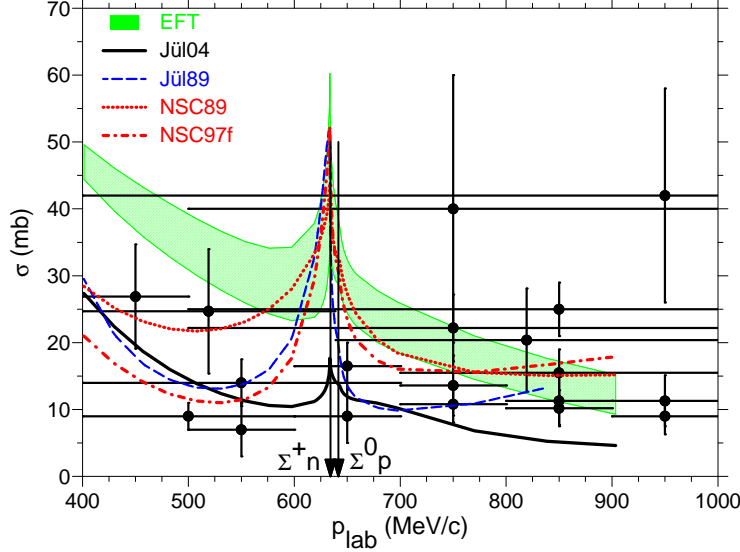

Figure 2: Cross sections for elastic Λp scattering. Data are from [2, 26–30]. The curves are results from YN models, namely from the Nijmegen YN soft-core potentials NSC97f [17] (dashed curve) and NSC89 [18] (dash-dotted curve), and from the Jülich one-boson-exchange models [15] (solid curve). and [16] (dashed curve). Results obtained at leading-order chiral EFT [19, 20] are indicated by the grey band. The thresholds for the reactions $\Lambda p \to \Sigma N$ are indicated by arrows.

Note that that the results in Fig. 1 are calculated in isospin basis using isospin-averaged Σ and nucleon masses. In particular, the ΛN momentum and the ΣN threshold are evaluated for $m_N = [m_p + m_n]/2$ and $m_\Sigma = [m_{\Sigma^+} + m_{\Sigma^0} + m_{\Sigma^-}]/3$, respectively.

Experimentally, in principle, the Λp interaction could be studied in the range of interest, i. e. in the vicinity of the ΣN thresholds by elastic scattering. In Fig. 2 all cross sections [2, 26–30] – to the best of our knowledge – for elastic scattering in a momentum range from 400 MeV/c to 1 GeV/c are collected. In addition to data we include the model calculations for the Nijmegen soft-core potentials NSC97f [17] and NSC89 [18], the Jülich meson-exchange models Jül05 [15] and Jül89 [16], and the leading-order chiral EFT interaction [19, 20].

Here the computation of the cross section was done in particle basis so that the $\Sigma^+ n$ and $\Sigma^0 p$ thresholds could be correctly implemented. Partial waves up

to $L \leq 2$ have been taken into account. Note that the agreement between data and calculations at low energies (not shown here) is of similar quality for all models.

Obviously, the data on elastic scattering are insufficient in quality to allow to discriminate between the different scenarios. It is therefore highly desirable to have additional data of high quality.

3 The reaction $K^-d \rightarrow \pi^- \Lambda p$.

One possibility to study the Λp interaction is via the *FSI* in reactions like $K^-d \rightarrow \pi^- \Lambda p$. In elastic scattering the contribution from the spin-triplet waves to the cross section can be expected to be the larger one due to its statistical weight. For the above reaction we expect likewise the main contribution to come from spin-triplet states and, specifically, from the $^3S_1$-wave, but due to different reason: the deuteron is already present in the initial state. For kaon absorption at rest the final baryonic state has to have predominantly the quantum numbers of the deuteron. At lowest order the reaction should be dominated by $K^-n \rightarrow \pi^-\Lambda$ (quasi-elastic) scattering leaving the spin-space part of the baryon state unchanged.

Fig. 3 shows the Λp spectra in the center-of-mass (c.m.) system. The data are taken from Refs. [4–7,9,10,31]. There is clearly a peak around the ΣN mass, i.e. around 2.13 GeV. However, the shape of the peaks as well as the underlying cross section vary from one experiment to the other. One reason for this are different boundary conditions in the experiments and the analysis. We will return to this point later. In order to study this dependence further we compare in more detail some of the spectra. The data from Sims *et al.* [7] are ignored since they have a poor signal to background ratio, i.e. do not allow to study the structure in detail. Similarly, the data from Alexander *et al.* [31] as well as those from Cline *et al.* [5] with bin widths of 10 MeV and poor statistics are excluded. The latter data have only two bins with 67 counts together in the peak region thus a width of the peak cannot be extracted. The data from Eastwood *et al.* [9] on the other hand contain some more counts (130) but in thirteen bins. We therefore kept these data. First we inspect the spectra from Tan [4] and Braun et al. [6]. These are data sets with rather large statistics. The smooth yield below the peaks contains, in addition to the direct reaction (2), contributions from the reaction with a heavier intermediate hyperon: $K^-d \rightarrow \Sigma^-(1385)p$ which decays in a second step as $\Sigma^-(1385) \rightarrow \Lambda\pi^-$. In order to avoid any phenomenological modelling and possible ambiguities associated with that we simply subtract some yield below the peak by fitting polynomials to these yields. We will discuss this further in section 5.3. The result is depicted in Fig. 4. Then this fitted cross section is subtracted from the experimental cross section so that only the peak structure remains. The peak in Tan's paper [4] shows a shoulder on the heavy mass side. In the case of the unconstrained data from Braun et al. [6] the structure looks quite different. There is much more yield to the high-mass side than in Tan's data. At this point we have to elucidate that
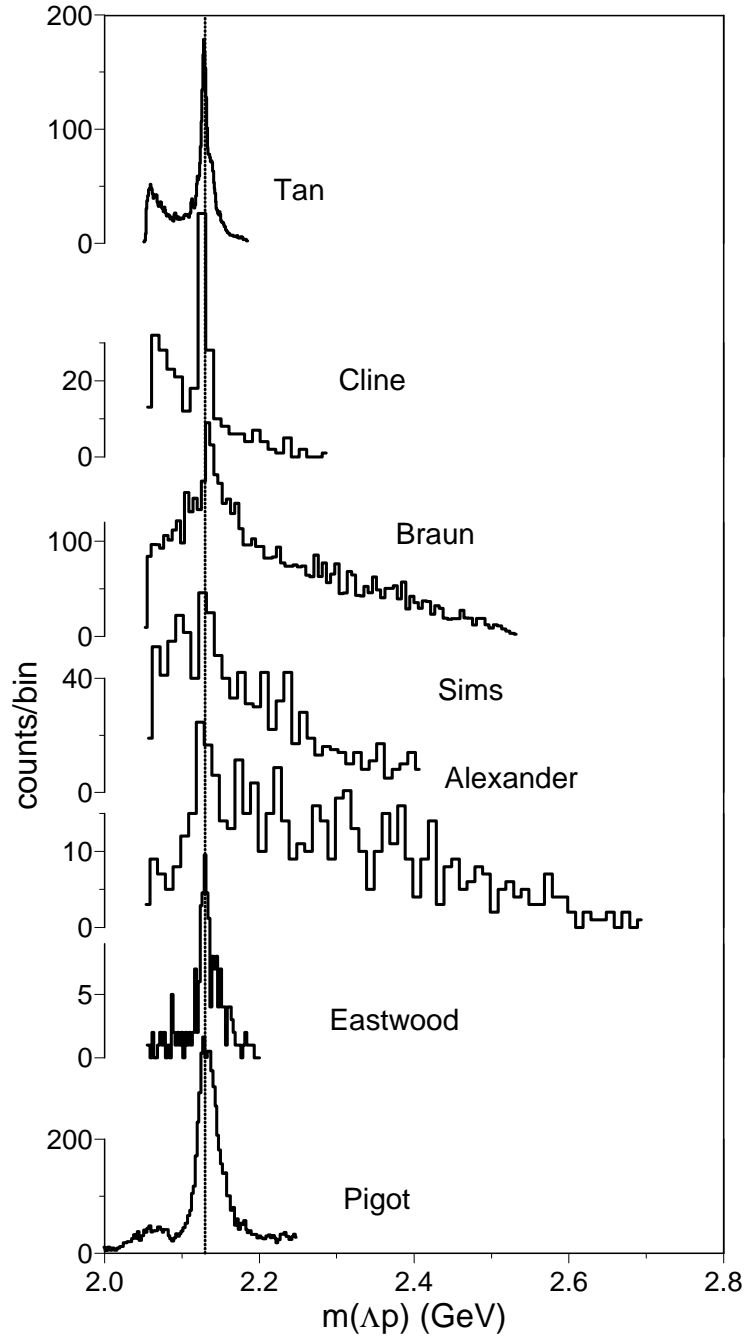
Figure 3: Invariant mass spectra for the reaction $K^- d \to \pi^- \Lambda p$. The data are from Tan [4], Cline *et al.* [5], Braun *et al.* [6], Sims *et al.* [7], Alexander *et al.* [8], Eastwood *et al.* [9], and Pigot *et al.* [10]. The dotted line indicates the averaged ΣN mass 2.13 GeV.
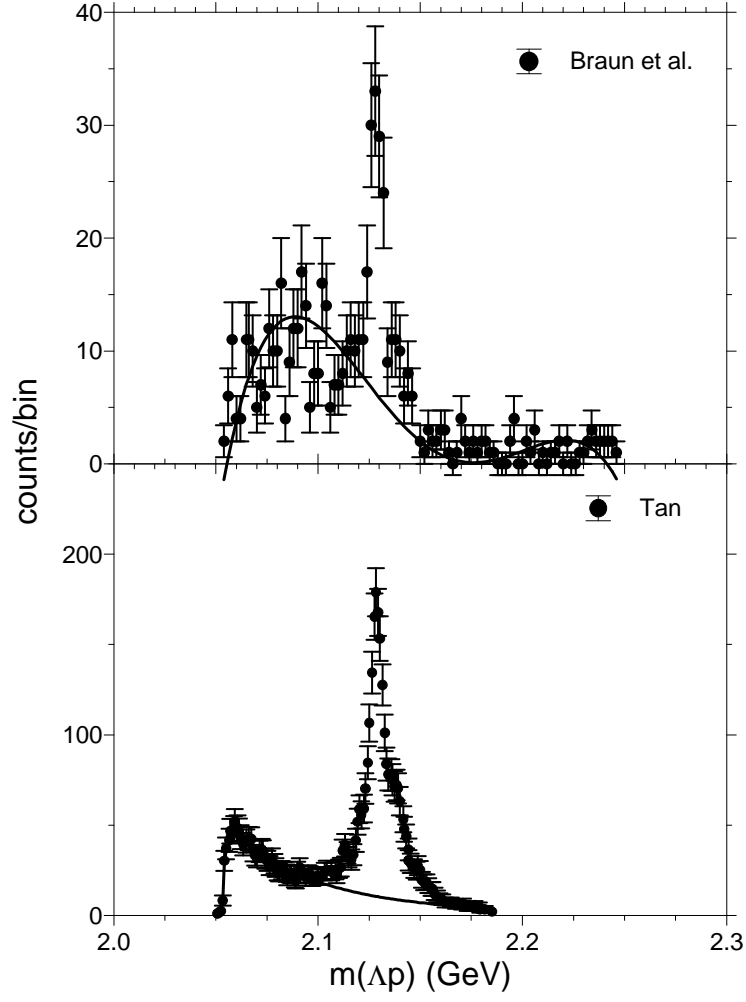
Figure 4: The missing mass spectra for the constrained data (see text) from [6] (upper panel) and [4] (lower panel). The solid curves show fits to the data where the peak region has been excluded.

9

this comparison is made between different things. The data from Braun *et al.* have no constraints while in case of Tan, counts with proton momenta below 75 MeV/c have been cut. Thus, reactions with the proton as a mere spectator $K^- d \to \pi^- \Lambda p_s$, with the two baryons being uncorrelated are excluded. In order to have really both hadrons in the entrance channel participating in the reaction Braun *et al.* introduced two cuts: (i) a threshold in the proton momentum of 150 MeV/c and (ii) the requirement of the angle between the incoming kaon and the outgoing pion $0.9 < \cos(K, \pi) < 1$. If one takes that into account the peak agrees, with respect to its shape and its position, to a large extent to the one reported by Tan [4] as is discussed in Sect. 5. Note that Eastwood *et al.* [9] required the proton momenta to be larger than 170 MeV/c.

While almost all groups relied on bubble chambers, Pigot *et al.* [10] applied a magnetic spectrometer to detect the emerging pions. However, most π^-'s are not from reaction (2) but from beam decays $K^- \to 2\pi^- \pi^+$. In order to reduce the number of such events the target cylinder was surrounded by twelve scintillation counters. After the decay of the Λ into two charged particles one has then three charged particles in addition to the forward going pion. Therefore, the authors studied the data with charged particle multiplicity $m \geq 2$ in these scintillators. For the width of the peak they give only upper limits. They also studied the line reversed reaction (3). The cross section for this reaction is smaller than for the strangeness exchange. Spectator protons are rarely detected in the set-up since they are stopped in the liquid deuterium target being 4 cm in diameter. Their final result is 2129±0.2±0.2 MeV and 16.7±1.9±2 MeV for the position and the width of the peak, respectively. Here we make use of their data set of the reaction (2) taken at a beam momentum of 1.4 GeV/c and multiplicity $m \geq 3$. For this case the spectrum is rather clean and the statistics is still sufficient – which is not the case for the other data sets. We then proceed as in the other cases. The final results for the structure at the ΣN threshold are given for all cases in Figs. 9 and 11.

4   The reaction $pp \to K^+ \Lambda p$

Most studies of the reaction $pp \to K^+ \Lambda p$ report only total cross sections. Hogan *et. al* [32] and more recently the COSY-TOF collaboration [33, 34] published spectra. However, these experiments although having rather large acceptances suffer from insufficient resolution to study a peak in the threshold region. These unfavorable boundary conditions were overcome with sufficient high resolution by Siebert et al. [11] employing the SPES4 spectrometer at Saclay and, more recently, even more by the HIRES experiment [12,35] making use of the Big Karl spectrometer [36] at the COoler SYnchrotron COSY Jülich. The disadvantage of the experiments from Refs. [11, 12, 32, 35] is that they are inclusive. This means that above the ΣN threshold also the $\Sigma^0 p$ and $\Sigma^+ n$ channels contribute to the experimental cross section. Thus a peak in the experimental spectrum is more difficult to see because the signal will be distorted by the rising contributions from the ΣN channels. Therefore, the following analysis is incomplete

and should be revisited upon future availability of good near-threshold $\Sigma - N$ production cross sections.

Already at first glance there are differences between reactions (2) and (4). For example, available data suggest that the peak to background ratio of the structure around the ΣN threshold is significantly smaller for the latter reaction. Furthermore, the detection of a kaon in the final state is much more delicate as compared to the detection of a pion, due to its short life time. One thing in common, after applying the cuts as discussed in the previous section, is that both baryons participate in the reactions.

Here we will first concentrate on the data from Refs. [11] and [12]. In these experiments the four momentum of the kaon was measured and the missing mass of the YN system was deduced. The missing mass resolution in the Saclay experiment [11] varied between 3 to 5 MeV (FWHM) depending on the angle while the HIRES experiments [35] and [12] reported a resolution of 0.8 MeV.

The bubble chamber measurements and the exclusive COSY-TOF data are projections from Dalitz plots and hence they are in the c.m. system. To make the other data comparable to them we transform them into the c.m. system.

The authors of Ref. [11] report about several energy shifts they have applied to their data. We shift the data back by two MeV in order that the steep rise of the cross section agrees with the threshold for the Λp channel. This is demonstrated in Fig. 5 where the shifted data are compared with calculated cross section

$$\frac{d^2\sigma}{dm d\Omega^*} \propto \Phi_3 \cdot F_{FSI} \tag{5}$$

with Φ_3 the three body phase space and F_{FSI} is the enhancement factor for the final state interaction from Ref. [35]. In order to show the effect of 2 MeV we have shifted this curve by two MeV up. This curve cannot account for the data points in the steep rise close to threshold (see insert in Fig. 5). The data close to the threshold agree well with FSI modified phase space. This Λp yield represented by Eq. (5) is then subtracted from the experimental spectrum. The remaining yield is then assumed to be due to the contributions from the $pp \to K^+\Sigma^+n$ and $pp \to K^0\Sigma^+p$ reactions, and from the structure of interest. Finally we subtract the cross section of the two Σ channels assuming $K^+\Sigma N$ being phase space distributed. This is also shown in Fig. 5.

The same procedure is applied to the HIRES data. The different steps are depicted in Fig. 6. By this method the structure close to the ΣN thresholds is extracted.

The new data from TOF [37] are exclusive. In general such data are superior to inclusive data since subtraction of cross sections due to other reactions is unnecessary. The spectra as function of the Λp mass were obtained by projection of the Dalitz plot onto this axis. The particles detected in the final state were K^+, p and the decay $\Lambda \to \pi^- p$. The first set of data labelled here by TOF I were taken at a beam momentum of 3.003 GeV/c while the second one was taken at 2.95 GeV/c. The resolution of the first set is 6 MeV after a kinematical fit while for the second 2 MeV is reported due to a new tracking system [38]. We proceed as before by fitting Eq. (5) to the data outside the peak region. This
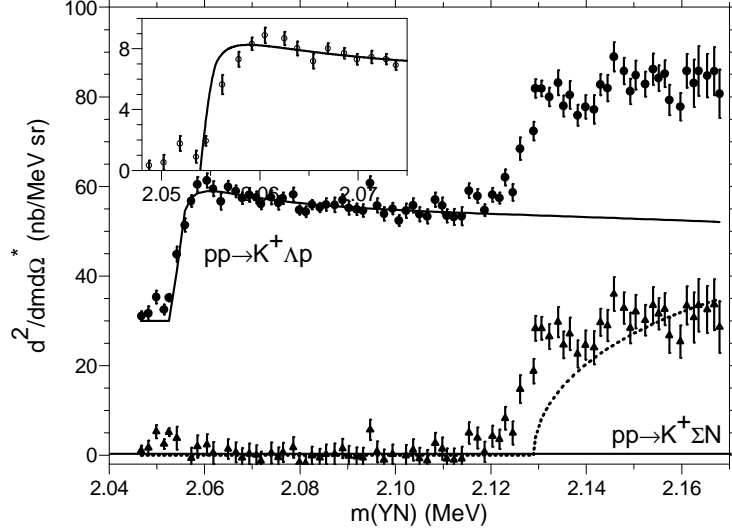
Figure 5: Upper curve: The data from SPES 4 (full dots) [11] at a lab. angle of (10±2) ^{o}. The beam had a momentum of 3.1 GeV/c. The data are transformed into the c.m. system and shifted by 5 nb/MeV sr in height and by 2 MeV down in the mass scale. The solid curve is the fit with Eq. (5) making use of the *FSI* parameters from Ref. [35]. The lower curve (full triangles) is the difference between the data in the upper curve and the fit. The short dashed curve is the fit of phase space for $\Sigma^+ n$. The insert shows again the solid curve (without the 5 nb/MeV sr shift and the data without the mass shift of 2 MeV.)

is shown for the TOF II data set in Fig. 7. This procedure accounts very well for the exclusive data. Especially the high mass side is well reproduced by pure phase space. We can still go a step further and compare the peak regions of the exclusive data with the inclusive data. This comparison is made in Fig. 8. There is a remarkable degree of similarity between the two results although the latter data are taken at a beam momentum 80 MeV/c higher than in the case of the HIRES data. The similar shape in the right side of the peak - except for $m(\Lambda p) \approx 2.1475$ GeV - contradicts the statement made in Ref. [39] that a large fraction of the cross section ascribed to the ΣN production might be Λp production.

At this point it might be appropriate to comment on that work further. First the authors state that "it is further hypothesised (in Ref. [12]) that, away from the near-threshold region, the differential cross section for $pp \to K^+ p\Lambda$ is essentially the same to the left and right of the ΣN threshold, in marked contrast even to the phase-space behaviour." Inspection of the figure in Ref. [39] shows that FSI was ignored when showing phase space dependence. This is in stark contrast to the experimental finding, as can be seen in Fig. 7, that including
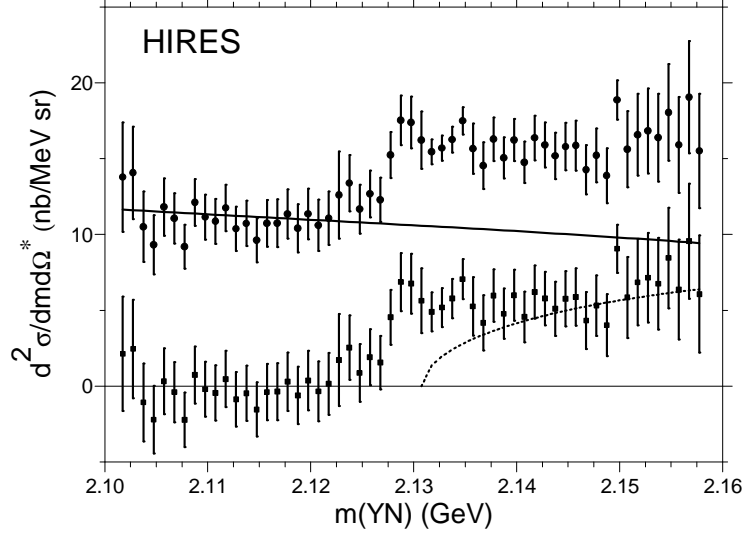
Figure 6: Same as Fig. 5 but for the HIRES data [12] measured around zero degree and at a beam momentum of 2.87 GeV/c.

FSI makes the shape of the cross section underlying the peak rather flat. This is even more pronounced for the study in the lab. system.

5 Analysis of the peak structure

Finally, Breit-Wigner distributions

$$\frac{d^2\sigma}{d\Omega_{K,\pi}dm_{\Lambda p}} = \frac{1}{\pi}\frac{d\sigma}{d\Omega_{K,\pi}}\frac{\Gamma/2}{(m(\Lambda p) - m_0)^2 - (\Gamma/2)^2} \tag{6}$$

were fitted to the different yields. Fit parameters were the width Γ and m_0, the centroid of the peak. The production cross section $d\sigma/d\Omega_{K,\pi}$ is also fitted. In Fig. 9 these fits were compared to the data. The deduced centroids and widths are shown in Fig. 9.

The fits yield a mean for the centroids $m_0 = 2130.3 \pm 0.6$ MeV and for the widths $\Gamma = 12.2 \pm 1.3$ MeV. There is a large scattering among the values and this is reflected by large χ^2/dof values. Especially the results for the data set TOF I are larger than the other values. This data set shows an asymmetric peak with a centroid at 2.132 ± 0.006 GeV [37]. When a symmetric peak is fitted the centroid moves further up to 2.1376 GeV. In particular, this is also in disagreement with the values extracted for the recent and more precise TOF II data. We, therefore, exclude these data from further analysis.

From inspection of the fits one gets the impression that the peak centroids are, with the exception of the data from Braun *et al.* [6], above the Σ^+n thresh-
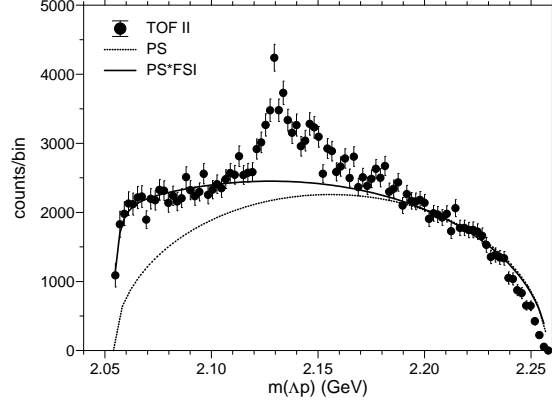
13

Figure 7: The exclusive cross sections for the reaction $pp \rightarrow K^+\Lambda p$ at 2.95 GeV/c from Ref. [37, 38]. The curves indicate the fit to the data outside the peak region. The solid curve is the fit with Eq. (5), the dashed curve is the pure phase space part.

old which is also indicated in Fig. 9. By way of example, Tan's data yield a centroid at 2129.55 ± 0.18 MeV and the peak width $\Gamma = 12.0 \pm 0.46$ MeV. The centroid is higher than in the analysis of Tan who reported 2128.7 ± 0.2 MeV. Also the width is much larger than the 7.0 ± 0.6 MeV reported by Tan. The reason is that he had fitted two Breit-Wigner functions to also account for a higher mass shoulder. We proceed by also fitting two Breit-Wigner distributions to all data. Then the peaks become smaller and there is good agreement between Tan's result and the one here. The agreement within errors shows the adequacy of the present method.

One feature of the data which has been also ignored so far is a shoulder in the peak distribution at higher missing masses. In order to take this shoulder into account we have fitted incoherently two Breit-Wigner forms to the data. These fits are - on a χ^2 criterion - slightly superior to those with only one Breit-Wigner. A fit on amplitude level did not indicate an interference. The peak region after subtraction of a smooth cross section fraction is shown for all data considered in Fig. 11.

Also shown are the fits with two Breit-Wigner functions. They account also for the higher mass range which was not in the case with a single Breit-Wigner (compare Fig. 9). The fits with two Breit-Wigner functions are also superior to those with only one Breit-Wigner on a χ^2 basis. This can be seen from the compilation in Table 1. The many values with $\chi^2/\text{dof}<1$ indicate that the authors have been very conservative in estimating the errors.

Obviously, there is a clear peak present in all data sets independent of the reaction. The shoulder visible for larger invariant masses appears also in all data sets. However, the latter looks somewhat different for the two reactions.
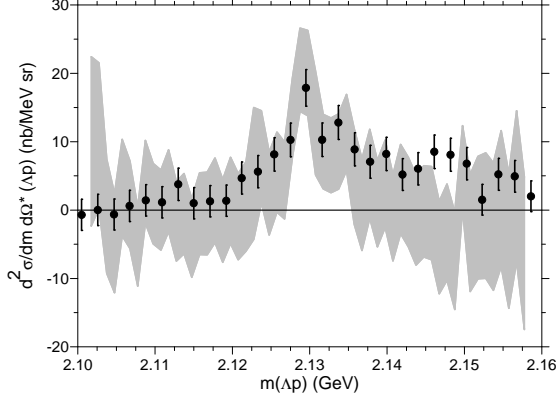
14

Figure 8: Comparison of spectral shapes in the peak region for the inclusive data from HIRES [12] and TOF [37,38]. The cross sections $d^2\sigma/dmd\Omega^*$ deduced for the HIRES data are shown as shaded area indicating the error band. The data $d\sigma/dm$ deduced from the TOF II data set divided by 300 are shown as full circles with error bars.

Table 1: The reduced χ^2-values obtained in the fits wit one Breit-Wigner (1 BW) and two Breit-Wigner forms (2 BW).

Ref.	χ^2/dof (1 BW)	χ^2/dof (2 BW)
Braun	0.64	0.63
Eastwood	0.92	0.58
Pigot	2.93	1.62
Tan	0.97	0.41
SPES4	1.5	1.2
HIRES	0.42	0.32
TOF II	1.63	1.0

The fit with two Breit-Wigner functions accounts well for the data sets in all cases.

The fit parameters for the two Breit-Wigner forms are visualized in Fig. 12. Again the values obtained for the data set TOF I are larger than all other results. The mean values and variances are also shown and given in Table 2. The values for the χ^2/dof indicate rather poor fits. For the lower-mass peak the centroids m_{01} scatter around the result for Tan's data. In all cases the fit parameters scatter. A plausible reason for this could be uncertainties in the beam momenta. However, then one would expect both centroids for a given measurement to be above or below the mean value. This is not the case. It should be mentioned that the second higher mass structure for the $pp \rightarrow K^+\Lambda p$ reaction is smaller than for the $K^-d \rightarrow \pi^-\Lambda p$ reaction. This may point to differences in the reaction mechanism for the two processes, which has to be
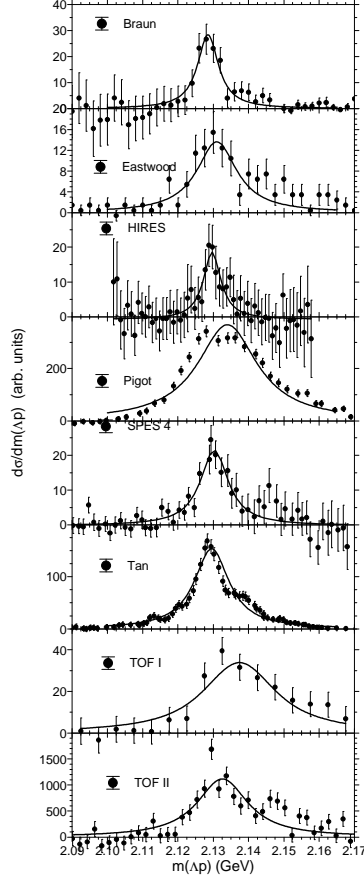
Figure 9: Data after subtraction of cross section with smooth behavior (for the $K^- d \to \pi^- \Lambda p$ reaction) or subtracted phase space distributions for $pp \to K^+ \Lambda p$ and $pp \to K^+ \Sigma^+ n$ as discussed in previous sections. The data (full dots with error bars) are from Braun *et al.* [6], Eastwood *et al.* [9], Pigot *et al.* [10], Tan [4], SPES 4 [11], HIRES [12], and TOF [37]. The data from [4, 6, 9, 10] are from strangeness exchange (2), the others are from associated strangeness production (4). Also shown are fits with a Breit-Wigner distributions (solid curves).
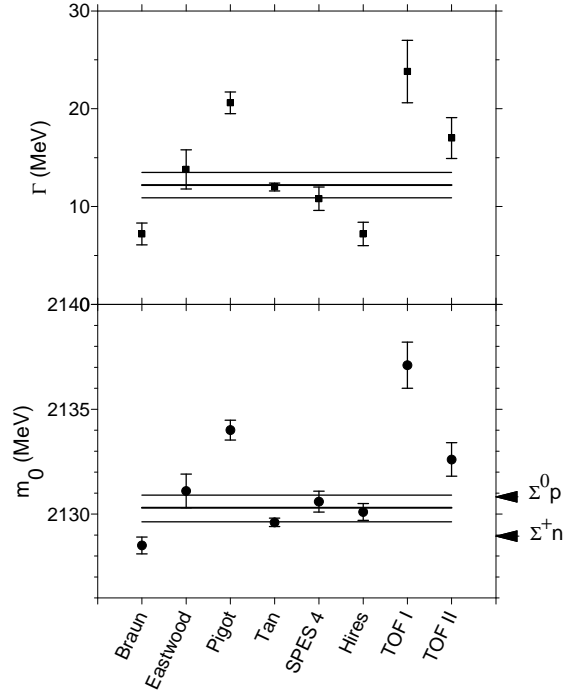
Figure 10: The fitted centroid values (lower panel) and widthes (upper panel) from the fits with one Breit-Wigner distribution for the data sets from Braun *et al.* [6], Eastwood *et al.* [9], Pigot *et al.* [10], Tan [4], SPES4 [11], HIRES [12], and TOF [37]. The lines show the mean (thick line) and its variance (thin lines). The arrows show the positions of the indicated thresholds.

expected anyway.

5.1 The lower-mass peak

We are now left with the question of what the origin of the structure is. We have shown above that the lower-mass peak position coincides with the $\Sigma^+ n$ threshold. This would hint to a genuine cusp effect [14]. However, the question arises to what precision the experimental missing masses are known. Possible shifts in the missing mass distributions in the bubble chamber measurements were minimized by studying the chamber magnetic field, energy range relation or kinematic fits to reference reactions. In the case of the kaon beam applied by Pigot et al. [10] the incident beam was carefully measured with the help of a magnetic spectrometer. In the proton-proton experiments the question reduces to the precision with which the accelerator beam momentum is known. In lower energy experiments at COSY Jülich employing the spectrograph Big Karl deviations of 0.11 to 0.5 MeV/c were found [36] and the COSY beam energy
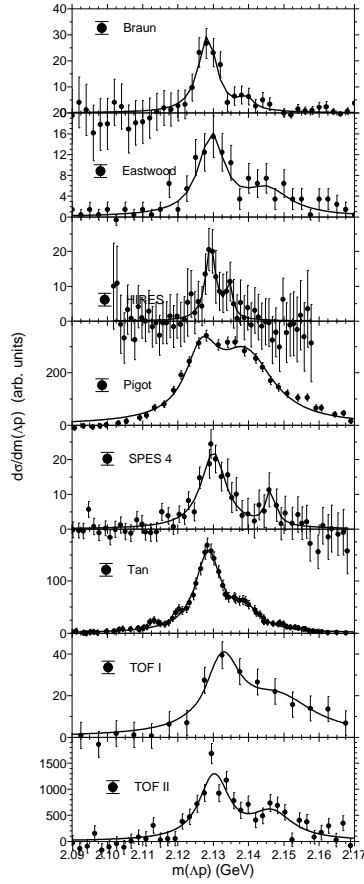
Figure 11: Same as Fig. 9 but for two Breit-Wigner distributions fitted to each data set.

in later experiments was corrected for these small deviations. Similarly for momenta around 1930 MeV/c a deviation of 2 MeV/c toward higher momenta was found [40]. Such a deviation by 2 MeV/c would amount to a shift up of 0.7 MeV for the HIRES experiment. However, no correction was found to be necessary when taking the Λp threshold as benchmark [35]. Note that the demanded agreement between the HIRES and the SPES4 data required a shift of the latter to the low energy side closer to the nominal accelerator beam momentum. From these findings we conclude that the energy scale in the data used here is reliable and therefore the lower-mass peak is at the $\Sigma^+ n$ threshold within two standard deviations of the experimental uncertainty. Thus, there is no evidence for a resonance in the Λp system below the ΣN threshold which in turn restricts the possibility of the existence of a strangeness $S = -1$ counterpart of the deuteron [41]. Of course, nothing can be said for the region within that
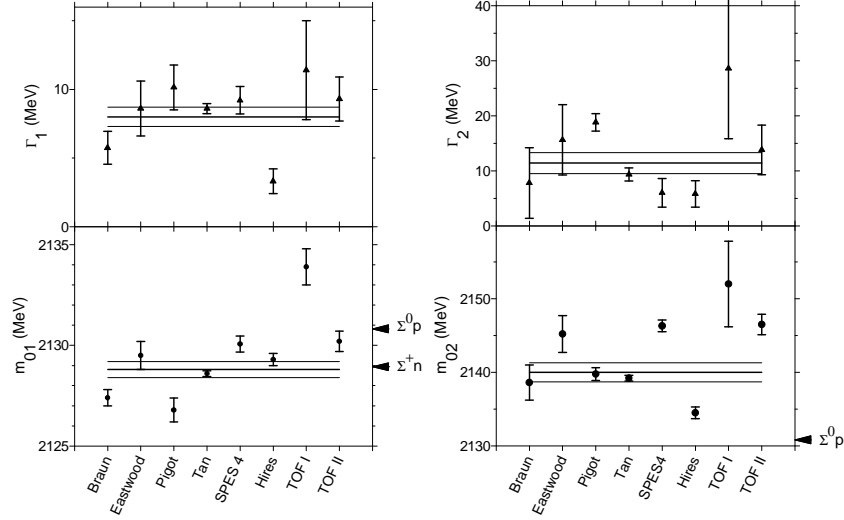
18

Figure 12: Same as Fig. 5. Left panel: The Breit-Wigner parameters for the low mass structure for the data sets from Braun *et al.* [6], Eastwood *et al.* [9], Pigot *et al.* [10], Tan [4], SPES4 [11], HIRES [12], and TOF [37]. The lines show the mean (thick line) and its variance (thin lines). The arrows show the positions of the indicated thresholds. Right panel; same as left panel but for the high mass structure. Note the wider scale on the right side compared to the left side.

uncertainty so that a quasi-bound deuteron-like state extremely close to the Σ^+n threshold cannot be excluded at present. We will study this possibility further.

5.2 Flatté approach

At this stage let us emphasize that the Breit-Wigner distributions are used here solely as a tool to determine the peak positions of the structures seen in the various experiments and to obtain values for the widths that can be compared with each other. They are not meant as a physical interpretation of the data. There are other parameterizations that are considered to be more adequate for amplitudes near a threshold like the one proposed by Flatté [42], specifically, if one wants to determine also the pole positions. However, those forms usually involve also more free parameters. Furthermore, the finite resolution of the experiment requires that the yield should be folded with Gaussians so that the functional form in the peak region would be identical anyway (see Braun et al. [6]).

In any case, we performed also exploratory calculations with the relativistic formulae of Flatté [42]. That the peak in Λp occurs just at the Σ^+n threshold

Table 2: The mean of the fitted Breit-Wigner distribution parameters excluding the TOF I data set. The centroids are denoted with $m_{0\mathrm{i}}$ and the widths with Γ_i.

variable	fitted value (MeV)	χ^2/dof
m_{01}	2128.7$\pm$0.3	8
Γ_1	8.0$\pm$0.7	6
m_{02}	2140.0$\pm$1.4	23
Γ_2	11.3$\pm$ 2.0	6

is no accident, if the production of the two hyperon-nucleon states are viewed as occurring via s-wave hyperon-nucleon scattering. As Flatté has pointed out then the drop on the high-mass side may be interpreted as the effect of the opening of the $\Sigma^+ n$ channel operating through unitarity. But the imposition of analyticity requires that the presence of the $\Sigma^+ n$ channel must be felt below threshold as well, thus creating the rapid decrease in the Λp cross section on the low-mass side of the peak. The differential cross section around the $\Sigma^+ n$ threshold is then

$$\frac{d\sigma_\nu}{dm} = C\left|\frac{m_r\sqrt{\Gamma_0\Gamma_\nu}}{m_r^2 - m^2 - im_r(\Gamma_1 + \Gamma_2)}\right|^2 \tag{7}$$

with $\nu = 1$ denoting $\Lambda p \to \Lambda p$ and $\nu = 2$ denoting $\Sigma^+ n \to \Lambda p$. The partial widths are

$$\Gamma_1 = \Gamma(\Lambda p \to \Lambda p) = g_1 k_1 \tag{8}$$

with g_1 an (effective) coupling constant squared [42] and k_1 the Λp c.m. momentum so that $m = \sqrt{m_\Lambda^2 + k_1^2} + \sqrt{m_p^2 + k_1^2}$. C denotes an overall normalization constant which includes the production cross section. m_r is the mass of the resonance and Γ_0 the partial width into the incoming channel. It is usually assumed to be weakly momentum dependent and thus can be assumed to be constant [42]. For the other channel we have

$$\Gamma_2 = \Gamma(\Sigma^+ n \to \Lambda p) = g_2 k_2 \tag{9}$$

with k_2 the $\Sigma^+ n$ c.m. momentum. Above the $\Sigma^+ n$ threshold k_2 is real but below the threshold it becomes purely imaginary so that

$$\Gamma_2 = \Gamma(\Sigma^+ n \to \Lambda p) = g_2 \kappa_2 \tag{10}$$

with $\kappa_2 = i|k_2|$. In this region the cross section is given by

$$\frac{d\sigma_1}{dm} = C\frac{m_r^2\Gamma_0\Gamma_1}{(m_r^2 - m^2 + m_r\Gamma_2)^2 + m_r^2\Gamma_1^2} \tag{11}$$

while $d\sigma_2/dm = 0$.

In the actual calculations we assumed that $\Gamma_0 = g_1 k_1(m_r)$. In practice, Γ_0 can be absorbed into the overall normalization factor C. It turned out

that the fits are not sensitive to the resonance parameters, something that was also seen already by Braun et al. [6] when analyzing their own data. Thus, it seems difficult to learn more on the pole position. Therefore, we kept those parameters fixed to reproduce a peak at the $(\Sigma^+ n)$ threshold and fitted only the other parameters (couplings and an overall normalization). In addition we assumed a Gaussian smearing with a fitted width to take into account the finite resolution of the different experiments. Although there is a large variation in the obtained values, the ratios of the coupling constants are better defined. Indeed, this is just a reflection of the scaling properties of the Flatté parametrization discussed in Ref. [45]. It is worthwhile to mention that the final curves due to the folding with the Gaussian resolution function are quite similar to Breit-Wigner functions.

The standard Flatté parametrization Eq. (7) produces only a single peak. It cannot generate the secondary peak (or shoulder) seen in the data. In order to account for this component we have coherently added a Breit-Wigner function. However, in the actual fit procedure the centroid of the Breit-Wigner is always moved to the maximum while simultaneously the Flatté part is reduced. The fits now show a wider distribution but with almost no interference. It should be stressed that the assumed Flatté formalism is only for a coupled two-channel system. In the discussed $\Lambda N - \Sigma N$ system there is also a tensor coupling between the $^3S_1$ and $^3D_1$ partial waves so that effectively, one deals with a system of four coupled channels and one would need to use a suitably generalized form for the Flatté parameterizations [3].

5.3 The higher-mass structure

In the case of the second structure, which in most of the data sets looks like a shoulder, there is no near-by threshold. Therefore one possible explanation is indeed that there could be a genuine resonance in the Λp system. However, such structures could be also artefacts of the cuts applied to the data from the $K^- d \to \pi^- \Lambda p$ reaction in order to exclude events from processes with the proton being a spectator. The momentum distribution of the nucleons in the deuteron is asymmetric with respect to its mean, say a Hulthén function with a maximum at 50 MeV/c. Energy cuts on the proton spectra in this order of magnitude were applied as discussed in Sect. 3. Deloff [43] showed that such cuts on the proton energy as well as on the proton emission angle affects the spectrum for $m(\Lambda p) < 2.1$ GeV. In order to study whether such cuts can produce structures in the spectra at higher mass values we perform Monte Carlo (MC) calculations. The quasi-free production is ignored. In addition to phase space the lower-mass peak is represented by a Breit-Wigner distribution (6) with $m_0 = m_{01}$ and $\Gamma = \Gamma_1$ the corresponding parameters from Table 2. A beam momentum of 760 MeV/c was chosen, which corresponds to the case of Ref. [6]. The Λp spectrum obtained in this way is shown in Fig. 13 as black curve. In a next step the requirement $p_p \geq 150$ MeV/c was chosen (red curve). The effect on the spectrum is minor. We then introduced the requirement $\cos(K^-, \pi^-) > 0.9$. This reduces the height of the spectrum severely with, however, no change in
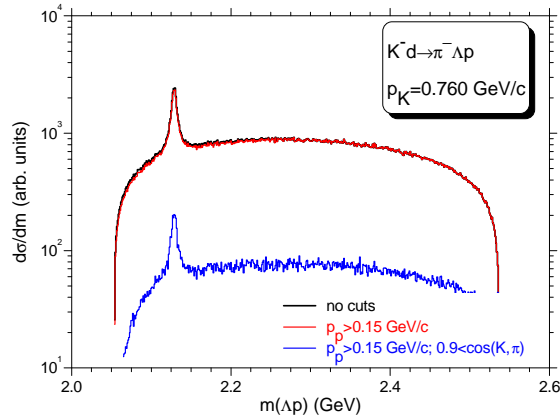
Figure 13: Monte Carlo calculations for the strangeness exchange reaction $K^-d \to \pi^-\Lambda p$ at a beam momentum of 0.760 GeV/c. A peak with Breit-Wigner shape for the peak with mass $m_0 1$ and width Γ_1 from Table 2 is added to phase space distribution. The spectrum without cuts is shown in black, with a cut on the proton momentum is shown in red and the one with an addition cut on the pion emission angle is shown in blue.

the spectral shape (blue curve). This is not surprising since below the peak there is phase space distribution and hence isotropic emission.

Another effect studied to inspect variations of the spectral shape are crossed-channel resonances. The Dalitz plot shown by Braun *et al.* [6] showed the excitation of the $\Sigma(1385)$ clearly. This resonance at the beam momentum of ≈ 760 MeV/c does not have an overlap with the peak at ≈ 2129 MeV. This is also visible in the Λp spectrum shown in Fig. 14. Resonance mass and width for that simulation are taken from the PDG [44]. A putative $\Sigma(1480)$ resonance (referred to as $\Sigma(1480)$ bumps by the PDG [44]) is not visible in the projection of the Dalitz plot on the $\pi^-\Lambda$ axis in [6]. Also such a resonance would not lie below the peak at 2129 MeV. The PDG [44] suggests in a note that there are two Σ resonances around 1670 MeV: a P_{11} at ≈ 1660 MeV with $\Gamma \approx 100$ MeV with three stars and a D_{13} at ≈ 1670 MeV with width $\Gamma \approx 60$ MeV with four stars. In order to account for these resonances we have assumed a mass of 1660 MeV and a width of 100 MeV. Although the Dalitz plot in [6] showed that the strengths of these resonances, if excited, are smaller than for the $\Sigma(1385)$, we assumed the same production cross section, since we are only interested in a possible change of the spectral shape. The peak area is clearly shifted up by the introduction of a such resonance, cf. Fig. 14, but the cross section below the peak remains smooth. Finally we examine the influence of crossed-channel resonances on data taken at kaon beam momenta almost at rest. This is shown in Fig. 15.

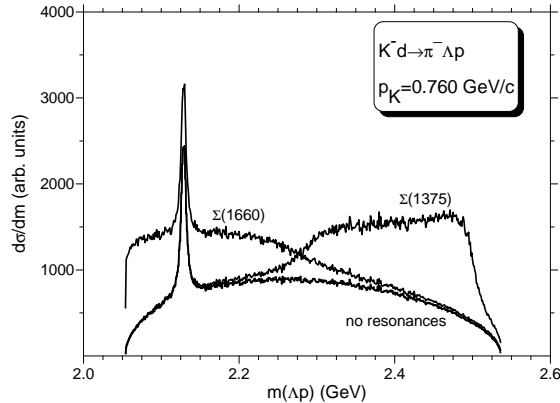A possible explanation for a shoulder at higher-mass was given in Toker *et*

Figure 14: MC calculation for the Λp spectrum for the reaction $K^- d \to \pi^- \Lambda p$ for a kaon momentum of 0.76 GeV/c. Influence of crossed-channel Σ resonances. Same description of the calculation as in Fig. 13.

al. [23]. In that work a shoulder was observed due to an interference between the "direct" Λ production mechanism and those involving the $\Sigma N \to \Lambda N$ transitions amplitude, in case of their interaction that produces an inelastic virtual state. We should add, however, that such a scenario was later on disputed by Deloff [43]. Rather, he advocated an interpretation that resorted to the presence of a P-wave resonance at 2140 MeV. In fact, enhanced P-wave contributions around the ΣN threshold are certainly possible. For example, an inspection of the $\Lambda p \to \Lambda p$ partial waves of the Jülich YN model, cf. Fig. 13 in [15], reveals the $^1P_1$-wave shows indeed some structure. As a consequence, there is a shoulder in the elastic scattering cross section at a few MeV above the ΣN threshold, see the solid line in Fig. 2. Its maximum is at 2139 MeV, when transformed to the Λp invariant mass, which is in good agreement with the experimental findings (see Table 2). However, the width is certainly larger than the experimental results.

The differences between the data for the two reactions are that the data from reaction $K^- d \to \pi^- \Lambda p$ are total cross sections whereas those for the $pp \to K^+ \Lambda p$ reaction are differential cross sections. Hence in the latter case interferences are possible which are absent in the first case. We study the second peak in the case of the second reaction further. Here we concentrate the discussion on the HIRES case. We may assume the second peak structure as a statistical fluctuation. A fit with only one Breit-Wigner yields $\chi^2/\text{dof}= 22.4/56$, while a fit with two Breit-Wigner functions yields 15/53. At this point it should be mentioned that the large error bars are not due to poor statistics but due to systematic uncertainties like flight paths in the spectrometer and decays along this path as well as uncertainties in the acceptance. Therefore a good fit does not yield $\chi^2/\text{dof}= 1$ as is the case of statistically distributed data. In a further
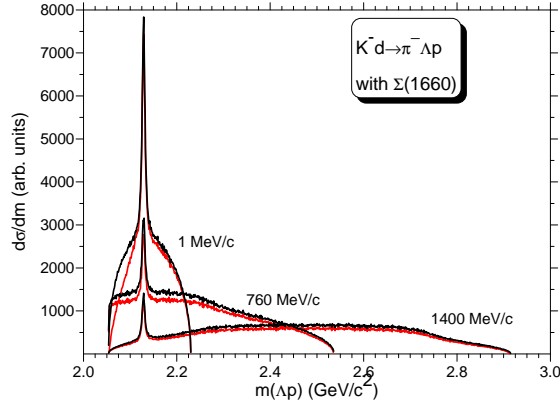
Figure 15: Same as Fig. 14 but for only $\Sigma(1660)$. The kaon beam momenta are next to the appropriate curves. The upper curves (black) are without cuts while the lower ones (red) are with cuts.

step we fit one Breit-Wigner by omitting the data in the range of the second peak. The remaining cross section was then fitted by a second Breit-Wigner. This is shown in Fig. 16 together with a fitted Breit-Wigner distribution. Note
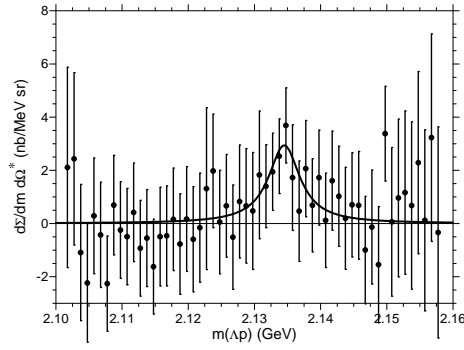

Figure 16: The remaining cross section after subtracting the low mass peak from the HIRES data. The solid curve is a fit with a Breit-Wigner function.

that the error bars contain the uncertainties from the different subtraction steps. The peak shows a significance of 4.0σ. This is smaller than the common practice of requiring 5σ for a discovery.

6   Summary and Discussion

We have studied the Λp interaction in the vicinity of the $\Sigma^+ n$ and $\Sigma^0 p$ thresholds. Experimental elastic transition cross sections do not show any particular enhancement at the threshold for the $\Lambda p \to \Sigma N$ scattering. However, the quality of the existing data is poor and does not allow for reliable conclusions. While the enhancement predicted by the recent Jülich OBE model [15] is modest, it is much larger in the Nijmegen soft-core potentials [17,18] and in the leading-order YN interaction obtained within the chiral effective field approach [19].

In the study of the Λp *FSI* in case of the strangeness exchange reaction $K^- d \to \pi^- \Lambda p$ the experiments made cuts of 75-150 MeV/c on the proton momenta, thus excluding real spectator protons. After applying the cuts the peaks at the ΣN thresholds from different experiments became comparable with respect to their shape. The influence of the momentum cuts as well as angular cuts were studied in detail by Deloff [43].

The enhancement is also visible in high resolution experiments employing the reaction $pp \to K^+ \Lambda p$. A good agreement is found with respect to the shape for those data from strangeness production Refs. [11,12] and [37]. When comparing the latter, where the data from Refs. [11] and [12] are transformed into the c.m system, with those from the reaction $K^- d \to \pi^- \Lambda p$, agreement is found for the structure around the ΣN threshold with cuts applied. This is expected since in the $pp \to K^+ \Lambda p$ reaction both nucleons participate due to π or K exchange. However, it seems mandatory to augment the $pp \to K^+ \Lambda p$ data when new exclusive measurements with high resolution close to threshold become available.

The coincidence of the peak maximum with the $\Sigma^+ n$ threshold within the experimental errors suggests that the peak is most likely due to a cusp effect induced by the strong coupling between the ΛN and ΣN channels. Some of the Nijmegen YN potentials produce a cusp in the $^3S_1 - ^3D_1$ partial wave [18,25]. The same is true for the recent Jülich model [15]. Conclusive evidence for an unstable (deuteron-like) bound state in the ΣN (isospin 1/2) channel, as predicted by other YN potentials in the literature [16,17], would require a peak that is well separated from the (and below the) $\Sigma^+ n$ threshold.

In both reactions there is a second peak at invariant masses well above the $\Sigma^0 p$ threshold. A possible interpretation due to deformation of the lower-mass peak by experimental cuts, crossed-channel resonances or interference effects can be excluded. Some YN potentials like the recent Jülich model [15] predict an enhanced P-wave contribution around the ΣN threshold, cf. the elastic $^1P_1$ phase shift in Fig. 13 of that reference. This leads to a shoulder in the Λp cross section in the relevant energy region, which at least qualitatively resembles the shoulder seen in the reactions discussed in the present study. But more exotic interpretations in form of a genuine Λp resonance are not excluded. For example, it might be a $S = -1$ state as predicted by Aerts and Dover [46,47]. However, their predicted $^1P_1$ state lies below the ΣN threshold. A recent review of $S = -1$ dibaryonic states can be found in Ref. [48].

Model calculations that study the enhancement seen in the Λp invariant

mass near the ΣN are all based on YN interactions that include the coupling between the ΛN and ΣN channels for obvious reasons [23, 41, 49, 50]. The investigations by Toker et al. [23] and Torres et al. [41] deal with the reaction $K^- d \to \pi^- \Lambda p$ and are performed in the Faddeev formalism. In Ref. [23] different potential models are employed that produce an inelastic virtual state (and thus a threshold cusp) but also an unstable bound state, where in the latter case a resonance-like behavior in the Λp cross section is generated slightly below and even above the threshold. No direct comparison of their results with the Λp spectrum of Tan [4] is presented. Torres et al. [41] achieve quantitative agreement with the data. They claim that a virtual state near the ΣN threshold is required for reproducing the data but not an unstable bound state. In the calculations for the associated strangeness production reaction (4) Deloff [49] as well as Laget [50] use YN interactions that produce a virtual state, namely the models presented in Ref. [43] in the former case and the Nijmegen model ND [24] in the latter.

New experiments with better statistics are required in order to discriminate between the different scenarios. Λ hyperons at low momenta could be produced with high intensity at the J-PARC facility in Japan and then used for pertinent experiments. Also the strangeness exchange reaction could be studied with the E31 setup again at J-PARC [51]. With regard to the $pp \to K^+ \Lambda p$ reaction exclusive data with full acceptance but even higher resolution than the existing ones would be highly desirable.

Acknowledgements

References

[1] R. H. Dalitz, B. W. Downs, Phys. Rev. 111 (1958) 967.

[2] G. Alexander, J. A. Anderson, F. S. Crawford, W. Laskar, L. J. Lloyd, Phys. Rev. Lett. 7 (1961) 348.

[3] A. M. Badalyan, L. P. Kok, M. I. Polikarpov, Y. A. Simonov, Phys. Rep. 82 (1982) 31.

[4] T. H. Tan, Phys. Rev. Lett. 23 (1969) 395.

[5] D. Cline, R. Laumann, J. Mapp, Phys. Rev. Lett. 20 (1968) 1452.

[6] O. Braun, H. J. Grimm, V. Hepp, H. Stroebel, C. Thoel, T. J. Thouw, F. Gandini, C. Kiesling, D. E. Plane, W. Wittek, Nucl. Phys. B 124 (1977) 45.

[7] W. H. Sims, J. S. O'Neal, J. R. Albright, E. B. Brucker, J. E. Lannutti, Phys. Rev. D3 (1971) 1162.

[8] G. Alexander, U. Karshon, A. Shapira, G. Yekutieli, R. Engelmann, H. Filthuth, W. Lughofer, Phys. Rev. 173 (1968) 1452.

[9] D. Eastwood, J. R. Fry, F. R. Heathcote, G. S. Islam, D. J. Candlin, G. Copley, G. R. Evans, J. R. Campbell, W. T. Morton, P. J. Negus, M. J. Counihan, D. P. Goyal, D. B. Miller, B. Schwarzschild, Phys. Rev. D 3 (1971) 2603.

[10] C. Pigot, et al., Nucl. Phys. B 249 (1985) 172.

[11] R. Siebert, et al., Nucl. Phys. A 567 (1994) 819.

[12] A. Budzanowski, et al. (HIRES Collaboration), Phys. Lett. B 692 (2010) 10.

[13] R. Newton, Scattering theory of waves and particles, McGraw-Hill, New York, 1966.

[14] K. Miyagawa, H. Yamamura, Phys. Rev. C 60 (1999) 024003.

[15] J. Haidenbauer, U.-G. Meißner, Phys. Rev. C 72 (2005) 044005.

[16] B. Holzenkamp, K. Holinde, J. Speth, Nucl. Phys. A 500 (1989) 485.

[17] T. A. Rijken, V. G. J. Stoks, Y. Yamamoto, Phys. Rev. C 59 (1999) 21.

[18] P. M. M. Maessen, T. A. Rijken, J. J. de Swart, Phys. Rev. C 40 (1989) 2226.

[19] H. Polinder, J. Haidenbauer, U.-G. Meißner, Nucl. Phys. A 779 (2006) 244.

[20] J. Haidenbauer, U. -G. Meissner, A. Nogga and H. Polinder, Lect. Notes Phys. **724** (2007) 113.

[21] M. M. Nagels, T. A. Rijken, J. J. de Swart, Phys. Rev. D 20 (1979) 1633.

[22] T. A. Rijken, Y. Yamamoto, Phys. Rev. C 73 (2006) 044008.

[23] G. Toker, A. Gal, J. M. Eisenberg, Nucl. Phys. A 362 (1981) 405.

[24] M. M. Nagels, T. A. Rijken, J. J. de Swart, Phys. Rev. D 15 (1977) 2547.

[25] T. A. Rijken, M. M. Nagels, Y. Yamamoto, Progress of Theor. Phys. Suppl. 185 (2010) 14.

[26] J. M. Hauptman, J. A. Kadyk, G. H. Trilling, Phys. Lett. B 125 (1977) 29.

[27] J. A. Kadyk, G. Alexander, J. H. Chan, P. Gaposchkin, G. H. Trilling, Nucl. Phys. B 27 (1971) 13.

[28] D. Cline, R. March, M. Sheaff, Phys. Lett. B 25 (1967) 446.

[29] F. S. Crawford, M. Cresti, M. L. Good, F. T. Solmitz, M. L. Stevenson, H. K. Ticho, Phys. Rev. Lett. 2 (1959) 174.

[30] G. Charlton, J. Badier, E. Barrelet, I. Makarovisch, J. Pernegr, J. Hubbard, A. Leveque, C. Louedec, L. Moscoso, D. Revel, Phys. Lett. B 32 (1970) 720.

[31] G. Alexander, B. H. Hall, N. Jew, G. Kalmus, A. Kernan, Phys. Rev. Lett. 22 (1969) 483.

[32] W. J. Hogan, P. A. Piroué, A. J. S. Smith, Phys. Rev. 166 (1968) 1472.

[33] S. Abd El-Samad, et al. (COSY-TOF Collaboration), Phys. Lett. B 632 (2006) 27.

[34] S. Abd El-Samad, et al. (COSY-TOF Collaboration), Phys. Lett. B 688 (2010) 142.

[35] A. Budzanowski, et al. (HIRES Collaboration), Phys. Lett. B 687 (2010) 31.

[36] M. Drochner, et al., Nucl. Phys. A 643 (1998) 55.

[37] S. Abd El-Samad, et al. (COSY-TOF Collaboration), arXiv nucl-ex (2012) 1206.0426.

[38] M. Röder, Final state interactions and polarization variables in the reaction $\vec{p}p \rightarrow pK^+\Lambda$ close to threshold, Ph.D. thesis, Ruhr-Universität Bochum (2011).

[39] Yu. Valdau, C. Wilkin, Phys. Lett. B 696 (2011) 23.

[40] M. G. Betigeri, et al. (The GEM collaboration), Nucl. Instrum. Methods Phys. Res. A426 (1999) 249.

[41] M. Torres, R. H. Dalitz, A. Deloff, Phys. Lett. B 174 (1986) 213.

[42] S. M. Flatté, Phys. Lett. B 63 (1976) 224.

[43] A. Deloff, Il Nuovo Cimento 102 A (1989) 217.

[44] K. Nakamura, et al. (Particle Data Group), J. Phys. G 37 (2010) 075021.

[45] V. Baru, J. Haidenbauer, C. Hanhart, A. Kudryavtsev, U.-G. Meißner, Eur. Phys. J. A 23 (2005) 523.

[46] A. T. M. Aerts, C. D. Dover, Phys. Lett. B 146 (1984) 95.

[47] A. T. M. Aerts, C. B. Dover, Nucl. Phys. B 253 (1985) 116.

[48] A. Gal, in: S. Lee (Ed.), From Nuclei to Stars: Festschrift in Honor of Gerald E Brown, World Scientific, Singapore, 2011.

[49] A. Deloff, Nucl. Phys. A 505 (1989) 583.

[50] J. M. Laget, Phys. Lett. B 259 (1991) 24.

[51] H.Noumi et al., http://www.j-parc.jp/researcher/Hadron/en/pac_1207/pdf/E31_2012-9.pdf